0.4 ± 0.3 and 0.6 ± 0.1, respectively. Preliminary indications are that the excited-state equilibrium is not established as rapidly in methanol and ethanol.

These and other preliminary results[26] indicate that pyridinium salts may very well serve as useful fluorescent probes for nucleic acids and perhaps other biomolecules. The pyridinium salt derived from hypoxanthine has a zwitterion which dominates the ground-state prototropic equilibrium at pH >6.7. It possesses a strong charge-transfer absorption band which is considerably red-shifted from the main UV absorption systems of the purines and pyrimidines. The excited zwitterion fluoresces moderately strongly, and the emission spectra and lifetimes are invariant over a wide pH range (3 < pH < 9 for PuPyCl), including the physiological region. This, together with the high degree of photostability of this particular system in aqueous solution, also suggests that it might find utility as a fluorescence standard. Preliminary work[26] indicates that other similar compounds may exhibit substantially larger fluorescence quantum yields. Transformation of hypoxanthine and other purine bases into pyrindium salts is straightforward.[7,8]

Experimental Section

Materials. *N*-Purin-6-ylpyridinium chloride was synthesized and purified according to the general procedure used previously for the synthesis of other nucleobase-derived pyridinium salts.[7,8] Thus, hypoxanthine (0.680 g, 5 mmol) was reacted with 4-chlorophenyl phosphorodichloridate (2.8 mL, 15mmol) to give 0.790 g of the desired compound. Yield: 68%. Mp >300 °C dec. MS: *m/e* (relative intensity) 197 (2.6) $(M - HCl)^+$, 79 (100) Py^+. NMR (D_2O): δ_H 10.03 (2 H, d, J = 5.8 Hz), 9.13 (1 H, s) 8.94 (1 H, t, J = 8 Hz), 8.80 (1 H, s), 8.43 (2 H, t, J = 7.5 Hz). Anal. Calcd for $C_{10}H_8N_5Cl$: C, 51.4; H, 2.3; N, 30.0. Found: C, 51.2; H, 2.4; N, 29.7.

$HClO_4$, $NaClO_4$, NaI, and D_2O were used as received. Spectrograde ethanol (Merck) and HPLC grade methanol and acetonitrile (both BDH Omnisolv) were used without further purification. Water was purified by using a Millipore Super-Q system. The samples used in the fluorescence measurements were prepared by volume from stock solutions of the fluorophore, $HClO_4$, NaI, and $NaClO_4$, so as to maintain a constant ionic strength.

Methods. The electronic absorption, excitation, and emission spectra were recorded on a Cary 118 spectrophotometer and a Spex Fluorolog 222 spectrofluorometer. All experiments, except for the temperature dependence of fluorescence in ethanol, were carried out at room temperature on aerated solutions. Fluorescence yields were determined relative to quinine bisulfate (ϕ_f = 0.55 1 N H_2SO_4[27]). A DN70 low-temperature cell and MT1C temperature control unit, both from Oxford Instruments, were used for fluorescence measurements between 293 and 77 K.

Fluorescence lifetime measurements were made on the picosecond laser system described previously[28] by using the single photon counting technique. The samples were excited at 297 nm, and emission was monitored at 461 and 521 nm, corresponding to the maxima in the deconvoluted emission spectra of the cation and zwitterion (Figure 4). Fluorescence decay curves were analyzed by the excitation pulse shape mimic technique developed earlier in this laboratory.[28] Th mimic chosen was 4-bromo-2,2,3,3-tetramethylindanthione in pentane (τ < 100 ps).[29] The χ^2 values were within 1.0–1.1 for single-exponential fits and did not exceed 1.3 for double-exponential decays. The errors for the lifetimes presented in this paper are no more than 3–5% for the longer-lived decays and are less than 15% for the short-lived components.

Acknowledgment. We thank the Natural Sciences and Engineering Research Council of Canada for financial support. B.S. thanks the President's NSERC fund of the University of Saskatchewan for providing the postdoctoral fellowship, A. Mickiewicz University for allowing a leave of absence, and Prof. S. Paszyc and Dr. R. W. Adamiak for their interest in this work. Partial support within the project R.P. II. 13.2.15 is also acknowledged.

(26) Skalski, B.; Steer, R. P.; Verrall, R. E.; Paszyc, S.; Adamiak, R. W. Proceedings, XIII International Conference on Photochemistry; Budapest, 1987; Abstracts; Vol. II, p 404.

(27) Demas, J. N.; Crosby, G. A. *J. Phys. Chem.* **1971**, *75*, 991.

(28) James, D. R.; Demmer, D. R. M.; Verrall, R. E.; Steer, R. P. *Rev. Sci. Instrum.* **1983**, *54*, 1121.

(29) Maciejewski, A.; Szymanski, M.; Steer, R. P., unpublished results.

H_xMoO_3 Bronzes: Structures, Stabilities, and Electronic Properties

S. P. Mehandru and Alfred B. Anderson*

Contribution from the Chemistry Department, Case Western Reserve University, Cleveland, Ohio 44106. *Received June 18, 1987*

Abstract: An atom superposition and electron delocalization molecular orbital study has been made of H° adsorption on MoO_3. Band structures, geometries, binding energies, force constants, and stretching frequencies have been calculated. It is predicted that H° adsorbs most strongly on the basal plane O^{2-} for the low as well as high hydrogen content H_xMoO_3 bronze. For the higher hydrogen content bronze, earlier suggestions in the literature that OH_2 groups are formed are confirmed. Once on the basal planes between the layers, hydrogen is expected to diffuse easily at high temperatures. On the edges of the crystal layers, the most stable chemisorption form is heterolytic, with H^+ bonded to O^{2-} and H^- bonded to Mo^{VI}.

A variety of bronzes, A_xMO_3 where M = W, Mo, Re and A = Na, K, Rb, Cs, NH_4, Ca, Sr, Ba, etc., are found to be superconductors with critical temperatures as high as 6 K.[1] Hydrogen bronzes have been used as heterogeneous catalysts for the hydrogenation of NO[2] and alkenes,[3] where they act as hydrogen reservoirs. Color changes often accompany bronze formation and this property has been investigated in connection with their use as electrochromic devices for displays.[4] The effect of hydrogen

(1) (a) Sweedler, A. R.; Raub, C.; Matthias, B. T. *Phys. Lett.* **1965**, *15*, 108. (b) Sweedler, A. R.; Hulm, J. K.; Matthias, B. T.; Geballe, T. H. *Phys. Lett.* **1965**, *19*, 82. (c) Bierstedt, P. E.; Bither, T. A.; Darnell, F. J. *Solid State Commun.* **1966**, *4*, 25. (d) Gier, T. E.; Pease, D. C.; Sleight, A. W.; Bither, T. A. *Inorg. Chem.* **1968**, *7*, 1646. (e) Sleight, A. W.; Bither, T. A.; Bierstedt, P. E. *Solid State Commun.* **1969**, *7*, 299.

(2) (a) Glemser, O.; Lutz, G. *Z. Anorg. Allg. Chem.* **1951**, *264*, 17. (b) Glemser, O.; Hauschild, U.; Lutz, G. *Z. Anorg. Allg. Chem.* **1952**, *269*, 93.

(3) (a) Sermon, P. A.; Bond, G. C. *Catal. Rev. Sci. Eng.* **1973**, *8*, 211. (b) Bond, G. C.; Sermon, P. A.; Tripathi, J. B. P. *Ind. Chim. Belge* **1973**, *38*, 506. (c) Sermon, P. A.; Bond, G. C. *J. Chem. Soc., Faraday Trans.* **1980**, *76*, 889. (d) Marcq, J. P.; Wispenninckx, X.; Poncelet, G.; Keravis, D.; Fripiat, J. J. *J. Catal.* **1982**, *73*, 309. (e) Marcq, J. P.; Poncelet, G.; Fripiat, J. J. *J. Catal.* **1984**, *87*, 339.

(4) (a) Chang, I. F.; Gilbert, B. L.; Sun, T. I. *J. Electrochem. Soc.* **1975**, *122*, 955. (b) Reichman, B.; Bard, A. J. *J. Electrochem. Soc.* **1979**, *126*, 2133. (c) Gottesfeld, S.; McIntyre, J. D. E. *J. Electrochem. Soc.* **1979**, *126*, 742, 2171.

0002-7863/88/1510-2061$01.50/0

in increasing the conductivity of TiO_2 photoanodes,[5] possibly by forming a bronze, has also been studied. Despite the catalytic and technological importance of hydrogen bronzes, the nature of hydrogen adsorption and absorption is poorly understood.

Hydrogen adsorbs heterolytically on surfaces of ZnO[6] and the alkaline-earth oxides MgO, CaO, and SrO.[7] It may be viewed as H^+ bonded to O^{2-} to form OH^-, and H^- bonded to the M^{2+} to form MH^+. Theoretical studies have recently explained why the heterolytic mode of adsorption is favored over the homolytic mode on ZnO surfaces, based on the electronic structure of the oxide.[8] The homolytically adsorbed H atoms on two O^{2-} sites are less stable because when two OH^- groups are formed, two electrons have to be promoted to the bottom of the metal conduction band or to the metal "dangling" surface orbitals, which lie about 2–3 eV above the filled O 2p band. The heterolytic mode of adsorption is favored because in this case no electron promotional energy is involved. Our recent molecular orbital studies of propylene adsorption on α-Bi_2O_3,[9] and methane adsorption on MoO_3,[10] $CuMoO_4$,[11] and MgO[12] have shown that these hydrocarbons also adsorb heterolytically on these oxide surfaces with H^+ on O^{2-}, and CH_3^- or $C_3H_5^-$ on the metal site. This is consistent with the earlier suggestion of Kokes and co-workers[13] that propylene chemisorbs to ZnO to form allylic intermediates bound to Zn^{2+}, and OH^-. The studies in references 10–12 also explain why O^- on the oxide surfaces activates methane CH bonds, but there is no evidence for O^- activation of hydrocarbon CH bonds or H_2 on ZnO.

MoO_3 has a band gap of about 3 eV between the filled O 2p and empty Mo 4d conduction bands.[14] It is made up of O^{2-}-covered sheets that are weakly bound together and cleave easily. Cation coordination sites are expected at edges of the sheets. On the basis of the reasons given above, H_2 adsorption on the edge sites of MoO_3 should be heterolytic with H^+ bonded to O^{2-}, and H^- bonded to Mo^{VI}. At ambient temperatures, MoO_3 is known to undergo topotactic reduction with hydrogen to form hydrogen–molybdenum bronzes, H_xMoO_3 ($0 < x \leq 2$). These are ternary oxide phases formed by the insertion of atomic hydrogen into the MoO_3 lattice. The reduction of MoO_3 can occur in aqueous acidic media by chemical[2] or electrochemical[15] methods. This can also be brought about by the spillover technique[16] whereby atomic hydrogen, produced by dissociating H_2 on platinum particles dispersed on MoO_3, diffuses into the oxide lattice, forming the bronze. Four distinct phases have been characterized with different hydrogen contents:[17] blue orthorhombic ($0.23 < x < 0.4$), blue monoclinic ($0.85 < x < 1.04$), red monoclinic ($1.55 < x < 1.72$), and green monoclinic ($x = 2$). The positions of the inserted hydrogen atoms and their interaction with the host lattice oxygens are not completely understood.

The purpose of the present theoretical study is twofold. First, we intend to predict the locations of the protons in the bulk H_xMoO_3 bronzes. There are three types of O^{2-} in MoO_3, but NMR and neutron diffraction work[18] does not clearly specify proton positions among them in the various bronze phases. Structures, stabilities, and other properties are calculated by using cluster models and the atom superposition and electron delocalization molecular orbital (ASED–MO) theory.[19] Second, we wish to determine whether heterolytic adsorption at layer edge sites is more stable than reductive homolytic adsorption on layer faces.

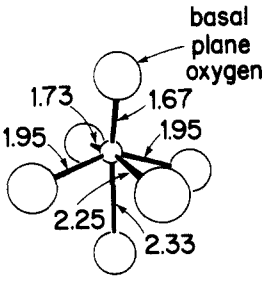

Figure 1. O^{2-} coordinations of Mo^{VI} in bulk MoO_3; bond lengths in Å. The small circle is Mo^{VI} and large circles are O^{2-}.

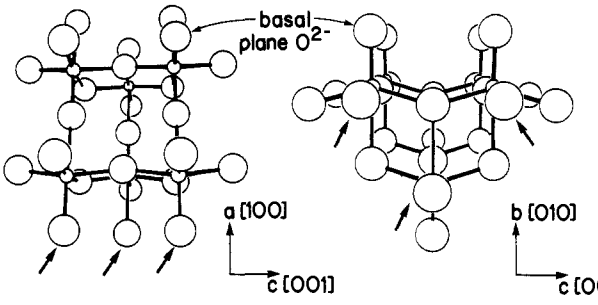

Figure 2. The $Mo_6O_{25}^{14-}$ cluster model used in some of the calculations, viewed from two different directions. Small circles are Mo^{VI} and the large circles are O^{2-}. The arrows indicate the three O^{2-} removed to form $Mo_6O_{22}^{8-}$ cluster containing three partially coordinated Mo^{VI} atoms on the (100) plane.

Table I. Atomic Parameters Used in the Calculations

atom	orbital	Slater exponent (au)	IP[b] (eV)
Mo	5s	2.256	9.10
	5p	1.956	5.92
	4d[a]	4.542 (0.5899)	10.56
		1.901 (0.5899)	
O	2s	1.946	26.48
	2p	1.927	11.62
H	1s	1.2	11.6

[a] Double-ζ with linear coefficients in parentheses. [b] IP = ionization potential.

Theoretical Method and MoO_3 Structure

The semiempirical ASED–MO method derives from partitioning the molecular electronic charge density function into an atomic part (a corresponding atom superposition energy is calculated from the atomic charge densities, and is repulsive) and an electron delocalization part (a corresponding electron delocalization energy is approximated as molecular orbital stabilization energy using a one-electron hamiltonian, and is attractive). A sum of the two parts gives a working approximation to

(5) (a) Chester, P. F.; Bradhurst, P. H. *Nature (London)* **1963**, *149*, 1056. (b) Ginley, D. S.; Knotek, M. L. *J. Electrochem. Soc.* **1979**, *126*, 2163.
(6) (a) Boccuzzi, F.; Borello, E.; Zecchina, A.; Bossi, A.; Camia, M. *J. Catal.* **1978**, *51*, 150. (b) Kokes, R. J. *Acc. Chem. Res.* **1973**, *6*, 226. (c) Eischens, R. P.; Plisken, W. A. *J. Catal.* **1962**, *1*, 80.
(7) (a) Coluccia, S.; Tench, A. J. *Proc. Int. Congr. Catal., 7th*, 1980, paper B35. (b) Coluccia, S.; Boccuzzi, F.; Ghiotti, G.; Morterra, C. *J. Chem. Soc., Faraday Trans. 1* **1982**, *78*, 2111. (c) Ito, T.; Sekino, T.; Moriai, N.; Tokuda, T. *J. Chem. Soc., Faraday Trans. 1* **1981**, *77*, 2181. (d) Ito, T.; Murakami, T.; Tokuda, T. *J. Chem. Soc., Faraday Trans. 1* **1983**, *79*, 913. (e) Ito, T.; Kuramoto, M.; Yoshioka, M.; Tokuda, T. *J. Phys. Chem.* **1983**, *87*, 4411. (f) Ito, T.; Yoshioka, M.; Tokuda, T. *J. Chem. Soc., Faraday Trans. 1* **1983**, *79*, 2277.
(8) Anderson, A. B.; Nichols, J. A. *J. Am. Chem. Soc.* **1986**, *108*, 4742.
(9) Mehandru, S. P.; Anderson, A. B.; Brazdil, J. F. *J. Chem. Soc., Faraday Trans. 1* **1987**, *83*, 463.
(10) Mehandru, S. P.; Anderson, A. B.; Brazdil, J. F.; Grasselli, R. K. *J. Phys. Chem.* **1987**, *91*, 2930.
(11) Ward, M. D.; Brazdil, J. F.; Mehandru, S. P.; Anderson, A. B. *J. Phys. Chem.* **1987**, *91*, 6515.
(12) Mehandru, S. P.; Anderson, A. B.; Brazdil, J. F. *J. Am. Chem. Soc.*, in press.
(13) Kokes, R. J.; Dent, A. L. *Adv. Catal.* **1972**, *22*, 1.
(14) (a) Hoppmann, G.; Salje, E. *Opt. Commun.* **1979**, *30*, 199. (b) Ivanovskii, A. L.; Zhukov, V. P.; Slepukhin, V. K.; Gubanov, V. A.; Shveikin, G. P. *J. Struct. Chem.* **1980**, *21*, 30.
(15) Schöllhorn, R.; Kuhlmann, R.; Resenhard, J. O. *Mater. Res. Bull.* **1976**, *11*, 83.
(16) Sermon, P. A.; Bond, G. C. *J. Chem. Soc., Faraday Trans. 1* **1976**, *72*, 730.
(17) Birtill, J. J.; Dickens, P. G. *Mater. Res. Bull.* **1978**, *13*, 311.
(18) (a) Dickens, P. G.; Birtill, J. J.; Wright, C. J. *J. Solid State Chem.* **1979**, *28*, 185. (b) Cirillo, A. C., Jr.; Ryan, L.; Gerstein, B. C.; Fripiat, J. J. *J. Chem. Phys.* **1980**, *73*, 3060. (c) Taylor, R. E.; Ryan, L.; Tindall, P.; Gerstein, B. C. *J. Chem. Phys.* **1980**, *73*, 5500. (d) Slade, R. C.; Halstead, T. K.; Dickens, P. G. *J. Solid State Chem.* **1980**, *34*, 183. (e) Marinos, C.; Plesko, S.; Jonas, J.; Tinet, D.; Fripiat, J. J. *Chem. Phys. Lett.* **1983**, *96*, 357.
(19) (a) Anderson, A. B. *J. Chem. Phys.* **1974**, *60*, 2477. (b) Anderson, A. B. *J. Chem. Phys.* **1975**, *62*, 1187.

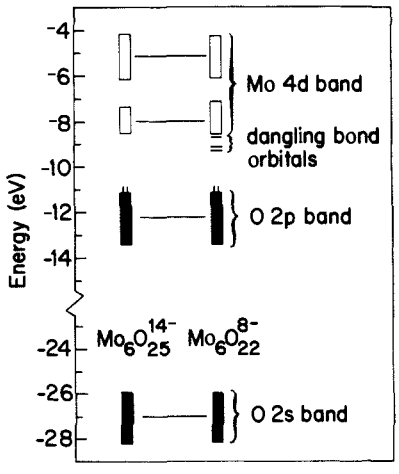

Figure 3. Electronic structures of the $Mo_6O_{25}^{14-}$ and the $Mo_6O_{22}^{8-}$ cluster models. Vertical bars represent electron occupations.

the bonding energy of the system. The method uses atomic valence state ionization potentials from the experimental literature and atomic Slater orbital exponents based on literature tabulations. The atomic parameters used in the present study are listed in Table I. For further discussion of the method and the origin and choice of these parameters, the reader is referred to ref 20.

Within each MoO_3 layer are distorted MoO_6 octahedra shown in Figure 1 (MoO bond lengths range from 1.67 to 2.33 Å) connected at two levels with sharing edges and corners as in Figure 2. The crystal belongs to the orthorhombic symmetry (a = 3.9628 Å, b = 13.855 Å, and c = 3.6964 Å).[21] Rigid bulk-superimposable cluster models are used for studying adsorption at basal plane O^{2-} and edge O^{2-} and Mo^{VI} sites in this work. Adsorbate bond distances reported in this paper are variationally optimized to the nearest hundreth of an angstrom and the bond angles to the nearest degree. The force constants are calculated by using energy and bond length differences in the formula $k_e = \Delta E^2/\Delta R^2$ (k_e is the harmonic stretching force constant, E is the system energy, and R is an internuclear distance).

Reductive Hydrogen Adsorption on MoO_3. Bronze Formation

As pointed out in the introduction, atomic hydrogen inserts into MoO_3 and forms H_xMoO_3 bronzes. X-ray powder patterns of these bronzes have shown that there is little crystallographic distortion of the MoO_3 lattice when hydrogen diffuses into the oxide lattice.[17,22,23] Powder neutron diffraction and inelastic neutron scattering investigations conducted by Dickens et al.[18a] have suggested that H is present as OH in the $H_{0.36}MoO_3$ phase. They have also proposed that it is located within the MoO_3 layer and is attached to 2-fold coordinated oxygen atoms. Furthermore, they could not unambiguously assign hydrogen positions in the higher hydrogen-content phases, but the model involving two hydrogen atoms bonded to the terminal oxygen atoms (i.e., OH_2 groups) was found compatible with the inelastic neutron scattering spectrum. NMR studies[18b-e] are inconclusive.

In bulk MoO_3 there are three types of O^{2-} to which H• can chemisorb: 1-coordinated basal plane (coordinated to one Mo^{VI} ion and 1.67 Å from it), 2-coordinated (the Mo–O–Mo configuration is approximately linear with the two Mo–O distances being 1.73 and 2.25 Å), and 3-coordinated (two Mo–O distances are 1.95 Å each and the third is 2.33 Å). We have calculated adsorption energies of H• to these three types, using the bulk superimposable cluster model, $Mo_6O_{25}^{14-}$ (see Figure 2), which contains six bulk-coordinated Mo^{VI} and eleven bulk-coordinated O^{2-}. The electronic structure of MoO_3 based on this finite-sized cluster is shown on the left of Figure 3. For more details about the calculated electronic structure of MoO_3 and its comparison with experiment, ref 20 may be consulted. The calculated properties of H• bonded to the three types of bulk-coordinated

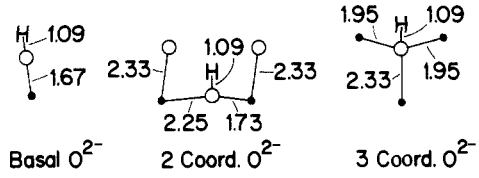

Figure 4. Predicted structures for H• atom adsorption on bulk-coordinated O^{2-} in MoO_3. Open circles represent O^{2-} and filled circles represent Mo^{VI}.

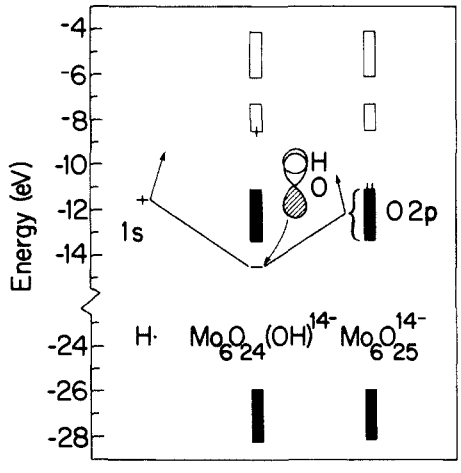

Figure 5. Molecular orbital correlation diagram and electronic structure for H• adsorbed on basal plane O^{2-} in MoO_3. Vertical bars represent electron occupations.

Table II. Calculated Bond Lengths, R_e (Å), Stretching Force Constants, k_e (mdyn/Å), Vibrational Frequencies, ω_e (cm^{-1}), and Dissociation Energies, D_0 (eV), for H• Binding to Various Bulk Coordinated O^{2-} in the $Mo_6O_{25}^{14-}$ Cluster Model

oxygen type	R_e	k_e	ω_e[a]	D_0[b]
basal O^{2-}	1.09	6.38	3394	2.03
2-coordinated O^{2-}	1.09	6.01	3294	1.33
3-coordinated O^{2-}	1.09	5.44	3134	0.28

[a] Diatomic approximation using k_e and omitting coupling to the bulk. [b] $D_e - {}^1/_2\omega_e$.

O^{2-} are given in Table II, and the structures are given in Figure 4. The binding of H• to the basal plane O^{2-} is favored over the binding to 2-coordinated and 3-coordinated O^{2-}. The OH distance is predicted to be the same for each type of O^{2-}, 1.09 Å, which is fortuitously the value deduced by Dickens et al.[18a] for 2-coordinated O^{2-} in the $D_{0.36}MoO_3$ bronze, though the present calculations indicate that the correct H binding site is the 1-coordinated O^{2-}. The calculated stretching force constants and the vibrational frequencies of H• bonded to the O^{2-} decrease with their increasing coordination. The energy level correlation diagram for H• adsorbed to the basal plane O^{2-} is shown in Figure 5. The H 1s and O 2p orbitals make a σ bond. The antibonding counterpart OH σ^* orbital is high up in energy and donates its electron into the lowest empty Mo 4d conduction band orbital, thus reducing the metal:

$$O^{2-} + Mo^{VI} + H^{\bullet} \rightarrow OH^- + Mo^{V}$$

The energetic expense of the electron promotion is what reduces this OH bond strength to about half of its value in diatomic OH. The binding energies in Table II are uncertain by several percent because of the nature of the model, and it may be noted that twice the basal OH D_0, 4.06 eV, is less than the H_2 D_0, which is 4.48 eV. This would imply that the hydrogen would not be stable in OH groups on the basal planes. The surface OH bond strength will be sensitive to the surface structure model and the ability of the ASED–MO method to produce proper band positions and a proper OH σ stabilization. Corrections to these could stabilize homolytic reductive H_2 adsorption. For example, it is noted the experimental D_0 value for diatomic OH, 4.39 eV, is 8% greater

(20) Anderson, A. B.; Kim, Y.; Ewing, D. W.; Grasselli, R. K.; Tenhover, M. *Surf. Sci.* **1983**, *134*, 237.
(21) Kihlborg, L. *Ark. Kemi* **1963**, *21*, 357.
(22) Kihlborg, L.; Hagerstrom, G.; Ronnquist, A. *Acta Chem. Scand.* **1961**, *15*, 1187.
(23) Wilhelmi, K.-A. *Acta Chem. Scand.* **1969**, *23*, 419.

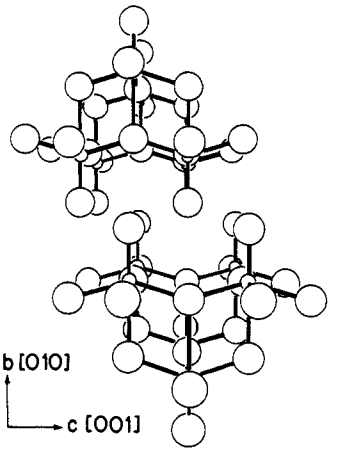

Figure 6. View of the $Mo_{12}O_{50}^{28-}$ cluster along the [100] direction. Small circles are Mo^{VI} and large circles are O^{2-}.

than the calculated value. An 8% increase in the calculated surface OH bond strengths would make homolytic reductive H_2 adsorption nearly stable.

To model the bronze phases containing higher hydrogen content we have employed a larger cluster, $Mo_{12}O_{50}^{28-}$, consisting of two MoO_3 layers stacked one above the other as in the bulk oxide. The side view of the edge and corner sharing MoO_6 octahedra along the [100] direction is shown in Figure 6. Each basal plane O^{2-} belonging to one sheet is surrounded by four basal plane O^{2-} at a distance of 2.82 Å belonging to the next layer. Since the terminal O^{2-} of one layer are separated by 3.24 and 3.65 Å from the 2-coordinated and 3-coordinated O^{2-} of the next layer, there should be sufficient room for hydrogen atoms to bind to the terminal O^{2-} without any repulsive interaction between the layers.

We allowed first one and then two H• to bind to each of the twelve basal plane O^{2-} in Figure 6. We have also allowed equal relaxations of these 12 O^{2-} along the bond directions before and after H• adsorption. The calculated terminal MoO bond lengths are 1.68 Å for the $Mo_{12}O_{50}^{28-}$ cluster compared to the experimental value of 1.67 Å in bulk MoO_3. When 12 H• were bonded to the terminal O^{2-}, one H• on each O^{2-}, and simultaneously relaxed, the MoO bonds lengthened by 0.07 Å each. The calculated OH distance of 1.09 Å is the same as that for a single H on the smaller cluster. The most stable configuration in our calculations has a MoOH angle of 180°. There is a possibility the angle is less than this because the ASED–MO method underestimates the ability of the lone-pairs on the oxygen to cause bending. With use of ω_e for basal O^{2-} in Table II, the calculated binding energy per H• is 1.90 eV. When 24 H• were bonded to the twelve basal plane O^{2-} to form OH_2 groups, each MoO bond length increased by 0.19 Å from the equilibrium value in MoO_3. In the most stable configuration, the two H• on each terminal O^{2-} point toward the 2-coordinated O^{2-} atoms belonging to the next layer. The calculated OH distances are 1.11 Å and the HOH angle is 107°. Removal of one of the water molecules is calculated to cost 1.70 eV. We obtain a binding energy of 2.11 eV per H• in this case, which is larger than the binding energy per H• when one H• binds on each of the terminal O^{2-}. From thermochemical data[24] binding energies in the range 2.7–2.9 eV can be deduced for the various bronze phases.

The cause for this increase in binding energy for two H• versus one H• on a terminal O^{2-} can be understood by focussing on Figure 7. This figure illustrates the electronic structures for the $Mo_{12}O_{50}^{28-}$ cluster, one H• per terminal O^{2-} on $Mo_{12}O_{50}^{28-}$, and two H• per terminal O^{2-} on $Mo_{12}O_{50}^{28-}$, including relaxations of the MoO bonds. In the case of $12H/Mo_{12}O_{50}^{28-}$, twelve OH σ bonding orbitals are formed with energies located below the O 2p band and 12 electrons have been promoted to the originally empty Mo 4d band. Because the orbitals in the Mo 4d band are antibonding between Mo and O, relaxations accompany their

(24) Birtill, J. J.; Dickens, P. G. *J. Solid State Chem.* **1979**, *29*, 367.

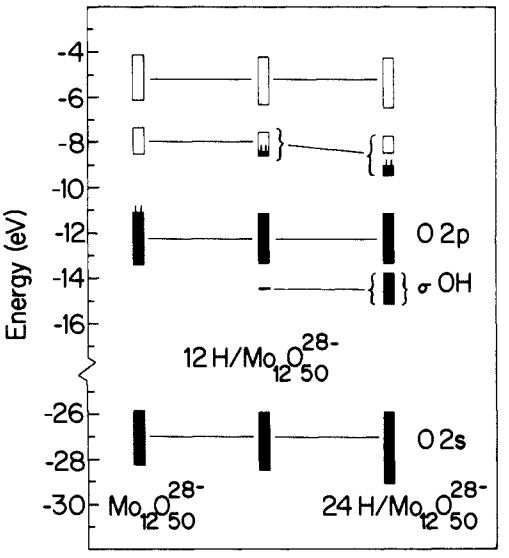

Figure 7. Electronic structures for one H• per basal plane O^{2-} and two H• per basal plane O^{2-} on the $Mo_{12}O_{50}^{28-}$ cluster. Vertical bars represent electron occupations.

occupation when H• adsorbs. As the 12 H• adsorb, the promoted electrons occupy increasingly higher energy orbitals so that the average binding energy per H• decreases. In the case of the $24H/Mo_{12}O_{50}^{28-}$ system, larger relaxations in the MoO bonds, which are due to the perturbation of the π metal–oxygen interaction, stabilize the Mo 4d energy levels substantially (see Figure 7). The promotional energy for the electrons is considerably smaller, which increases the average binding energy per H•, though from the thermochemical data[24] the average binding energy would be expected to decrease. It is generally believed[18a,d] that the OH_2 groups are in terminal positions, and the present calculations indicate this should be the most stable possibility.

We have calculated the barrier to H• diffusion over the O^{2-} basal plane using the cluster shown in Figure 6 and assuming that the saddle point is located in the middle of the two fixed-position O^{2-} between which the motion takes place. The possibility of proton tunneling is not included in the present analysis. The barrier to mobility is minimum (1.1 eV) when H• travels from one terminal O^{2-} belonging to one layer to another terminal O^{2-} belonging to the next layer. This provides a zigzag path for hydrogen mobility between layers. NMR studies[18d] have produced effective barriers of a few tenths of an electron volt for proton mobility in MoO_3.

Homolytic versus Heterolytic H_2 Adsorption on Edge Sites

In order to maintain stoichiometry, edges of small uncontaminated crystallites of oxides would terminate in adsorption sites with partially coordinated Mo^{VI} and O^{2-}. For example, it has been well established[7,25] that in rock-salt structure MgO, SrO, and CaO powders, there exist sites of unusually low coordinations, such as might be found at steps, edges, or corners, which give rise to photoluminescence with light of a much lower frequency than that expected from the band gap of bulk oxides. Such light absorption has been assigned to three surface state bands corresponding to the corner, the edge, and face Mg^{2+} sites in order of increasing energy for MgO.[12,25b] For stoichiometric MoS_2, which has a layered structure, low-coordination edge Mo^{IV} and S^{2-} have been considered in a recent ASED–MO study[26] of hydrogen adsorption. For the same reasons, coordinatively unsaturated Mo^{VI} and O^{2-} will exist at edges of MoO_3. Such coordinatively unsaturated edge sites are generally believed to be more reactive and are likely to

(25) (a) Zecchina, A.; Lofthouse, M. G.; Stone, F. S. *J. Chem. Soc., Faraday Trans. 1* **1975**, *71*, 1476. (b) Coluccia, S.; Deane, A. M.; Tench, A. J. *J. Chem. Soc., Faraday Trans. 1* **1978**, *74*, 2913. (c) Coluccia, S.; Barton, A.; Tench, A. J. *J. Chem. Soc., Faraday Trans. 1* **1981**, *77*, 2203.

(26) Anderson, A. B.; Al-Saigh, Z. Y.; Hall, W. K. *J. Phys. Chem.*, in press.

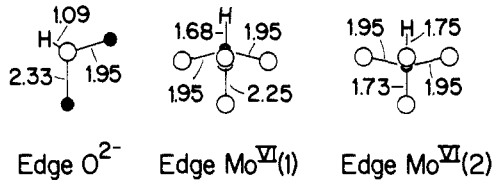

Figure 8. Calculated structures for H• adsorbed on the edge O^{2-} and Mo^{VI} sites on the $Mo_6O_{22}^{8-}$ cluster model. Open circles are O^{2-} and filled circles are Mo^{VI}.

Table III. Calculated Properties for H• Binding to Various Edge Sites on the $Mo_6O_{22}^{8-}$ Cluster Model[d]

site[a]	R_e	k_e	ω_e[b]	D_0[c]
basal O^{2-}	1.09	6.39	3397	3.12
edge O^{2-}	1.09	6.21	3348	3.08
edge Mo^{VI} (1)	1.68	2.97	2258	2.52
edge Mo^{VI} (2)	1.75	1.98	1843	1.26

[a] See Figure 8. [b] Diatomic approximation using k_e and omitting coupling to the bulk. [c] $D_e - {}^1/_2\omega_e$. [d] See title to Table II for the definition of the symbols.

participate in the initial steps of reactions occurring on these materials.

To calculate the reactivity of edge sites toward hydrogen adsorption, we removed three O^{2-}, indicated by arrows, from the fully coordinated cluster (Figure 2) to form the (100) surface of MoO_3. The calculated electronic structure based on the resulting $Mo_6O_{22}^{8-}$ cluster is shown on the right-hand side of Figure 3. The partially coordinated Mo^{VI} cations give rise to dangling bond orbital energy levels that lie between the bulk valence and conduction bands. The calculated results for H• bonding to various edge atoms on the $Mo_6O_{22}^{8-}$ cluster model are given in Table III and structures are given in Figure 8. The most favored binding site is the basal plane O^{2-}. Adsorption on the 1-coordinated edge O^{2-} is the same in energy. H• binds more strongly on the basal plane O^{2-} with an edge Mo^{VI} nearby than when in the bulk (3.12 and 2.03 eV, respectively). The cause for this increased binding energy is that the promoted electron goes to the Mo^{VI} surface orbital in the former case, which lies about 1 eV lower than the bottom of the bulk conduction band. For studying H• adsorption on the coordinatively unsaturated (5-fold coordinated) cations on the $MoO_3(100)$ surface, we have considered two types of Mo^{VI} that are likely to be present on the surface. Type 1 Mo^{VI} are those that are missing an O^{2-} that was 1.73 Å away in the bulk and type 2 Mo^{VI} are those that are missing an O^{2-} at a distance of 2.25 Å. As shown in Table III, H• binds much more strongly to type 1 Mo^{VI}. When H• binds to an edge Mo^{VI}, a σ bond forms as shown in Figure 9. Formally, the hydrogen atom becomes H^- by stealing an electron from the O 2p band.

When two H• adsorb homolytically on the basal plane O^{2-} sites with edge Mo^{VI} nearby, the net result is $2OH^- + 2e^-$. The total

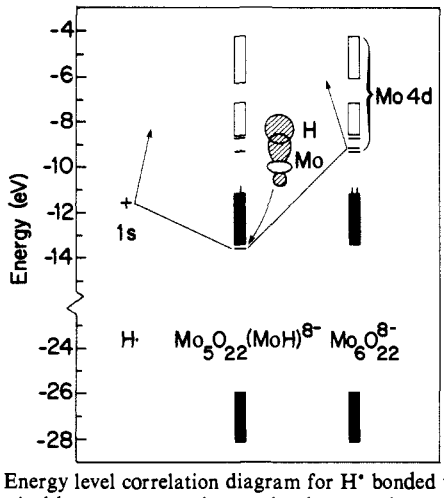

Figure 9. Energy level correlation diagram for H• bonded to a surface Mo^{VI}. Vertical bars represent electron level occupations.

binding energy is 6.24 eV. When H_2 adsorbs heterolytically, formally it becomes H^+ bonded to O^{2-} and H^- bonded to Mo^{VI}. Starting with the energies for H• adsorption on the terminal O^{2-} and type 1 Mo^{VI} and taking into account the energy of electron transfer within the cluster band structure, a heterolytic adsorption energy of 7.27 eV is found. Within the present model it appears that heterolytic adsorption products will be more stable on the edges of MoO_3, a result that is similar to the earlier results for ZnO[8] and MoS_2[26].

Concluding Comments

We have shown that edge sites of MoO_3 exposed to hydrogen activity are likely to be saturated with Mo^{VI}–H^- and adjacent O^{2-}–H^+ bonds. Reductive homolytic products, while stable relative to H_2, are less stable than the above heterolytic products. However, their stability is sufficient to allow hydrogen bronze formation when H• are introduced to the basal planes, as is observed experimentally.[2,15,16] As more H• cover the basal plane O^{2-} (adsorption to intralayer O^{2-} is not sufficiently stable), their average adsorption energies decrease slightly due to the progressive occupation of the Mo 4d conduction band. OH_2 formation is expected when the x value in H_xMoO_3 surpasses 1. Once OH_2 forms on the basal plane, it binds strongly enough that its removal and the reduction of Mo^{VI} will require a high temperature. In many ways these results parallel those for hydrogen adsorption on MoS_2,[26] which is also layered.

Acknowledgment. We thank the Standard Oil Company (now BP America, Inc.) and the NASA Lewis Research Center, through a grant to the Case Center for Electrochemical Sciences, for supporting this work.

Registry No. H, 12385-13-6; MoO_3, 1313-27-5.